Sequences flanking the transmembrane segments facilitate mitochondrial localization and membrane fusion by mitofusin

Xiaofang Huang[a,b], Xin Zhou[a,b], Xiaoyu Hu[a,b,1], Amit S. Joshi[c], Xiangyang Guo[a,b], Yushan Zhu[a,b], Quan Chen[a,b,d], William A. Prinz[c], and Junjie Hu[a,b,e,f,2]

[a]Department of Genetics and Cell Biology, College of Life Sciences, Nankai University, Tianjin 300071, China; [b]Tianjin Key Laboratory of Protein Sciences, Nankai University, Tianjin 300071, China; [c]Laboratory of Cell and Molecular Biology, National Institute of Diabetes and Digestive and Kidney Diseases, National Institutes of Health, Bethesda, MD 20892; [d]State Key Laboratory of Membrane Biology, Institute of Zoology, Chinese Academy of Sciences, Beijing 100101, China; [e]National Laboratory of Biomacromolecules, Center for Excellence in Biomacromolecules, Institute of Biophysics, Chinese Academy of Science, Beijing 100101, China; and [f]University of Chinese Academy of Sciences, Beijing 100101, China

Edited by Peter J. Novick, University of California, San Diego, La Jolla, CA, and approved October 5, 2017 (received for review May 26, 2017)

Mitochondria constantly divide and fuse. Homotypic fusion of the outer mitochondrial membranes requires the mitofusin (MFN) proteins, a family of dynamin-like GTPases. MFNs are anchored in the membrane by transmembrane (TM) segments, exposing both the N-terminal GTPase domain and the C-terminal tail (CT) to the cytosol. This arrangement is very similar to that of the atlastin (ATL) GTPases, which mediate fusion of endoplasmic reticulum (ER) membranes. We engineered various MFN-ATL chimeras to gain mechanistic insight into MFN-mediated fusion. When MFN1 is localized to the ER by TM swapping with ATL1, it functions in the maintenance of ER morphology and fusion. In addition, an amphipathic helix in the CT of MFN1 is exchangeable with that of ATL1 and critical for mitochondrial localization of MFN1. Furthermore, hydrophobic residues N-terminal to the TM segments of MFN1 play a role in membrane targeting but not fusion. Our findings provide important insight into MFN-mediated membrane fusion.

membrane fusion | membrane targeting | mitochondria | endoplasmic reticulum | mitofusin

Mitochondria are double membrane-bound organelles that govern ATP production and many other important cellular processes. Mitochondrial membranes undergo frequent fusion to maintain a ribbon-like morphology and actively divide for clearance of damaged portions or redistribution during cell division (1–3). These membrane dynamics are tightly regulated to ensure proper mitochondrial functioning. Mitochondrial fusion and fission are mediated primarily by dynamin-like proteins (DLPs) (4). In mammals, mitofusin (MFN) (Fzo1p in yeast) fuses outer mitochondrial membranes (5–7), and OPA1 (Mgm1p in yeast) merges inner mitochondrial membranes (8, 9), whereas Drp1 (Dnm1p in yeast) controls mitochondrial fission (10).

Among the DLPs, the MFN family was the first to be identified and suggested as membrane remodeling factors (11). MFN/Fuzzy Onion/Fzo1p proteins localize to the outer membrane of mitochondria, and their deletion causes fragmentation (12), indicating a lack of membrane fusion. Two MFN isoforms have been identified in mammalian cells (5). Both MFN1 and MFN2 are ubiquitously expressed and essential during embryonic development (13), but they exhibit distinct activities in mediating fusion (14). Mutations in MFN2 cause the neurodegenerative disease Charcot–Marie–Tooth Type 2A (CMT2A) (15), and the mitochondrial morphology regulated by MFN proteins has been linked to several critical physiological functions, including cardiomyocyte differentiation (16, 17), hematopoietic stem cell maintenance (18), spermatogenesis (19), and neuron-controlled energy metabolism (20, 21). MFN-mediated mitochondrial fusion is thought to be regulated by membrane potential (22), phosphorylation (23, 24), ubiquitination (25–27), acetylation (28), and numerous interacting proteins, such as MIB, MARCH-V, Gβ, Bax, and GPAT (29–33). Given the difficulties purifying and reconstituting MFN proteins, their sufficiency for membrane fusion is unclear.

MFNs comprise an N-terminal cytosolic GTPase followed by a helical bundle (HB) domain, a transmembrane (TM) domain, and a cytosolic C-terminal tail (CT). Two heptad repeats (HRs) have been predicted to reside in the HB and CT. MFNs are thought to localize in the mitochondrial membranes via the TM domain. However, deletion of the HB or CT of MFN2 results in the diffusion of some proteins into the cytosol (22), suggesting that the mitochondrial targeting of MFN is determined by multiple sequence elements. How MFN mediates mitochondrial fusion is also poorly understood. GTPase activity is known to be required (14, 22). The crystal structure of the CT of MFN1 revealed homotypic interactions in the form of an antiparallel coiled coil (34), suggesting that this region of MFNs (the second predicted heptad repeat, HR2) promotes the tethering of apposing mitochondrial membranes before fusion. Recent structural analysis of the minimal GTPase domain (MGD) of MFN1 revealed that membrane tethering is likely achieved

Significance

Mitochondria constantly connect through membrane fusion. The merging of the outer mitochondrial membrane requires mitofusin (MFN) proteins. MFN is a membrane-anchored GTPase, but whether it is sufficient to achieve fusion, and if so how, is largely unknown. We have taken advantage of a similar GTPase named atlastin (ATL), which mediates fusion of the endoplasmic reticulum (ER), as its mechanism is better understood. Domain swapping experiments show that MFN is capable of fusing membranes, even on the ER. The C-terminal tail of MFN contains an amphipathic helix that promotes fusion. MFN is properly inserted into the mitochondrial membrane with the help of the helix and neighboring hydrophobic residues. These findings provide insight into how mitochondria fuse.

Author contributions: X. Huang, X.Z., Q.C., W.A.P., and J.H. designed research; X. Huang, X.Z., X. Hu, A.S.J., and X.G. performed research; X. Huang, X.Z., X. Hu, A.S.J., Y.Z., and J.H. analyzed data; and J.H. wrote the paper.

The authors declare no conflict of interest.

This article is a PNAS Direct Submission.

[1]Present address: Department of Pharmacology, University of Texas Southwestern Medical Center, Dallas, TX 75390.

[2]To whom correspondence should be addressed. Email: huj@ibp.ac.cn.

This article contains supporting information online at www.pnas.org/lookup/suppl/doi:10.1073/pnas.1708782114/-/DCSupplemental.

through its GTP-dependent dimerization (35, 36). Cryo-EM tomography studies using isolated mitochondria confirmed that tethering/docking is GTP-dependent (37). Whether other regions of MFN contribute to the fusion activity remains to be investigated.

Another class of dynamin-like GTPases that mediates fusion of endoplasmic reticulum (ER) membranes has been identified: atlastin (ATL) in mammals, Sey1p in yeast, and RHD3 in plants (38–41). ATL and MFN are functionally analogous and share the same domain structure and membrane topology. The fusion mechanisms of ATL and Sey1p are better understood than those of MFN proteins. The crystal structure of the cytosolic domain of human ATL1 has been determined in three different conformations (42–44). In all structures, the GTPase domain of ATL forms a dimer, but the following three-helix bundle (3HB) docks to GTPase in either the same or the paired ATL molecule, orienting different directions relative to the GTPase dimer. A fusion model has been proposed in which GTP binding induces interactions between ATL molecules across the apposing membranes, and subsequent GTP hydrolysis causes conformational changes to force the HBs of engaging ATL molecules to come very close, pulling the two membranes together. In addition, the CT of ATL forms an amphipathic helix that binds and perturbs the membrane bilayer, facilitating the fusion process, and the TM segments are required for efficient fusion, probably via mediation of the nucleotide-independent oligomerization of ATL molecules (45). Structural and biochemical studies of Sey1p have revealed a conserved mechanism with some unique features (46).

Here, we elucidate how MFN mediates homotypic membrane fusion based on our knowledge of ATL. We show that the role of the MFN-CT appears to be different from that previously proposed. An amphipathic helix in the CT is critical for MFN-mediated fusion. Furthermore, the same helix and a loop region in the HB play a role in localizing MFN onto the outer mitochondrial membrane.

Results

Construction and Localization of MFN-ATL Chimeras. We generated MFN-ATL chimeras to determine whether MFN or ATL retain membrane fusion activity when they are relocated to a different organelle and whether MFN domains function similarly to their ATL counterparts. To ensure surgical precision in construction of the chimera, we performed a detailed sequence analysis of human MFN1. Overall, the secondary structures of MFN1 predicted by the "PredictProtein" program (47) exhibited a pattern very similar to that observed experimentally for human ATL1 and MFN1 (Fig. 1*A* and Fig. S1). The N-terminal MGD of MFN1 is composed of a classical GTPase and HB that is complemented by α11b from the CT. Three helices, numbered α7 to α9, were predicted between the MGD and TM segments of MFN1. We named this region the HBM domain (Fig. 1*A*, M for MFN1), and it is likely the second HB of MFN1, given that MGD already possesses one 4HB (35, 36). The previously defined HR1 (residues 373 to 400) is within α7. The TM segments of MFN1 (TMM) appear to be 33 residues in length, which was confirmed by online software TMHMM (www.cbs.dtu.dk/services/TMHMM/) and is considerably shorter than a conventional two-pass TM region, even if it forms a hairpin. The CT of MFN1 (CTM) was predicted to be extensively α-helical (including α10, α11a, and α11b). The latter two helices were previously known as HR2 and have appeared as one long helix in the crystal structure (34). Collectively, these analyses suggest that MFN1 can be divided into four parts: GM (1–361), HBM (362–595), TMM (596–628), and CTM (629–741) (Fig. 1*A*). Similarly, the corresponding parts of ATL1 have been defined as the following: GA (1–338), HBA (339–447), TMA (448–496), and CTA (497–558) (Fig. 1*A*, A for ATL1).

To relocate MFN or ATL, we switched their TM segments, the key targeting element for an integral membrane protein. For clarity, we named all of the chimeras used here according to the identity of their TM domain; chimeras containing TMA are designated as A-type and chimeras containing TMM are designated as M-type.

To move MFN1 to the ER, we created chimera A1 (GTPase^{MFN1}-HB^{MFN1}-TM^{ATL1}-CT^{MFN1} or GM-HBM-TMA-CTM). Immunofluorescence and the MitoTracker signal showed that A1 properly localized to the ER, but not the mitochondria, even though the mitochondrial morphology is slightly altered (Fig. 1*B*), possibly due to interactions between A1 and MFN1 (Fig. S2). In addition, A1 was found mostly in the tubular ER and very little protein was seen in peripheral ER sheets or the nuclear envelope, a feature reminiscent of ATL1 (Fig. 1*B*). To rule out the possibility that some of A1 remains on the mitochondria, we expressed A1 in MFN1-deleted mouse embryonic fibroblast (MEF) cells and monitored the mitochondrial morphology. A1 appeared as an ER pattern and, similar to untransfected cells, A1-expressing cells exhibited fragmented mitochondria (Fig. S3), suggesting a lack of A1 on mitochondria. Finally, deletion of the HBM (A2, GM-TMA-CTM) or CTM (A3, GM-HBM-TMA) from A1 did not alter the ER localization (Fig. S4*A*). These results indicate that the TMA is sufficient for localization of MFN1 to the ER.

When the TM domain of ATL1 was replaced with that of MFN1, the resulting mutant M1 (GA-HBA-TMM-CTA) did not localize to the mitochondria as expected; instead, it remained on the ER and exhibited dispersed distribution in the cytosol in some cells (Fig. 1*C* and Fig. S4*C*). Consistently, expression of M1 resulted in little rescue of defective mitochondrial morphology in MFN1-deleted MEF cells (Fig. S3). Truncation of the HR1- or HR2-containing regions in MFN2 has been shown to cause protein redistribution into the cytosol (48). We confirmed these findings using MFN1 protein lacking the newly defined HB (including HR1) or CT (including HR2) (Fig. S4*B*). Thus, the TMM is likely necessary, but not sufficient, for outer mitochondrial membrane targeting.

Functional Tests for MFN-ATL Chimeras Localized in the ER. We then tested the function of relocated MFNs. As the cytosolic domains of these MFN-containing chimeras could potentially interact with endogenous MFNs, we used a *Saccharomyces cerevisiae* system in which such cross-talk is less likely due to sequence divergence between ectopically expressed MFN mutants and endogenous Fzo1p (the yeast ortholog of MFN). To determine the activity of MFN localized in the ER, we analyzed whether MFN-ATL chimeras can replace Sey1p, a functional ortholog of ATL. Yeast cells lacking Sey1p and either Yop1p or Rtn1p, proteins that shape the ER tubules (49, 50), exhibited abnormal cortical ER morphology; in particular, the tubular ER network largely disappeared, and many areas of the cortex were void of ER, indicating a lack of ER fusion (39). These defects can be restored by the expression of wild-type (WT) Sey1p or human ATL1 (38, 39). When HA-tagged A1 was transformed into *sey1Δyop1Δ* cells using a CEN vector with the endogenous *SEY1* or*FZO1* promoter, no expression was detected (Fig. S5*A*). The levels of these chimeras became detectable only when using a high copy 2μ vector with a GAL promoter (Fig. S5*A*) and were equivalent to that of human ATL1 expressed under the endogenous *SEY1* promoter in a CEN vector (Fig. S5*A*). To confirm the localization of these chimeras in yeast cells, GFP-tagged chimeras were expressed in *sey1Δ* cells and compared with the localization of ER-targeted red fluorescent protein (RFP) (ss-RFP-HDEL). All A-type chimeras localized to the ER (Fig. S5*B*) as in mammalian cells.

To test whether some chimeras also localize to mitochondria and influence their morphology, we expressed A1 in *fzo1Δ* cells, in which mitochondria are fragmented. As observed with MFN-deleted MEF cells, A1 expression in yeast cells did not affect the mitochondrial morphology (Fig. S5*C*). Finally, we also

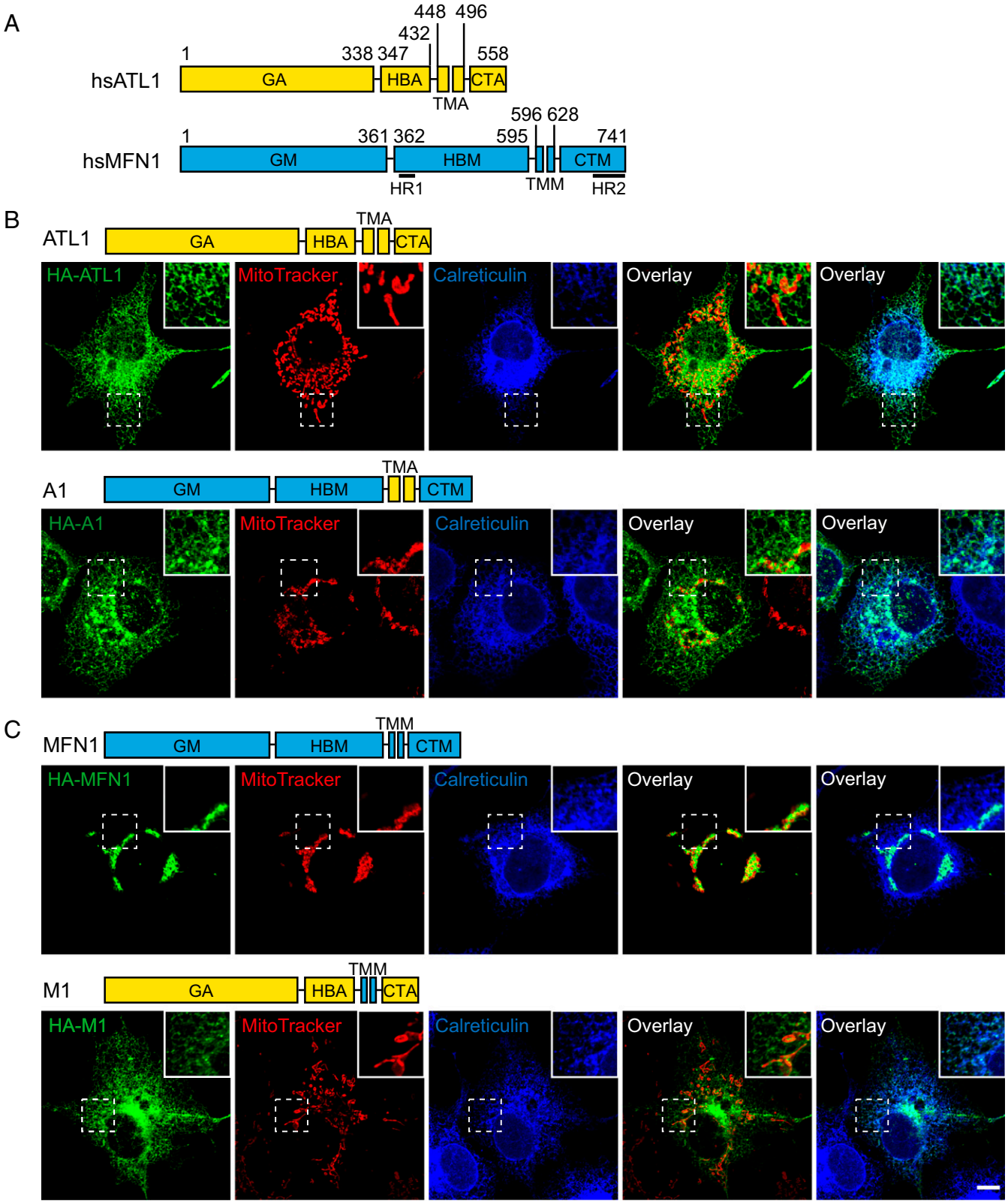

Fig. 1. Localization of MFN-ATL chimeras. (*A*) The domain structures of human ATL1 and MFN1 are shown in yellow and cyan, respectively. The first letter of each domain label represents the molecule (A for ATL1 and M or MFN1), and the following letters represent the domain type (CT, C-terminal tail; G, GTPase; HB, helix bundle; TM, transmembrane segments). The residue numbers used in constructing the chimeras are listed, and the predicted HR1 and HR2 of MFN1 are highlighted. hs, *Homo sapiens*. (*B*) HA-tagged chimeras that contain the ATL-TM domain were expressed in COS-7 cells. Localization was investigated using anti-HA antibodies (green) and compared with endogenous luminal ER protein, calreticulin (blue), or MitoTracker (red) by indirect immunofluorescence and confocal microscopy. The domain structures of the indicated chimeras are shown above the images. (*C*) As in *B*, but with cells expressing HA-tagged chimeras containing the MFN-TM domain. The *Insets* in *B* and *C* show the 2× enlargement of the indicated areas. (Scale bar for *B* and *C*: 10 μm.)

expressed A1 in *sey1Δyop1Δ* cells and observed no changes in mitochondrial morphology (Fig. S5*D*). These results confirmed that ATL1-TM efficiently redirects MFN1 to the ER, even in yeast cells.

The cortical ER of *sey1Δyop1Δ* cells expressing the chimeras was visualized by Sec63p-GFP. To better evaluate the ER morphology, we added a category of partially normal ER in which some fenestrated ER was observed, but areas of the cortex lacked ER (Fig. 2*A*). We found that, when A1 (GM-HBM-TMA-CTM) was expressed, a substantial number of cells had normal ER morphology (Fig. S5 *E* and *F*). In contrast, when the GTP-binding mutant A1 K88A was expressed, the ER morphology defects were not rescued (Fig. S5*E*). The ER defects were also retained with the expression of A2 (GM-TMA-CTM) and A3 (Fig. S5*E*). In addition, when MFN1 lacking HB or CT was transfected into MFN1-deleted MEF cells, mitochondria fragmentation was not restored (Fig. S3). Taken together, these results suggest that MFN1 is functional on the ER, with the HBM and CTM playing roles in fusion.

The CT of ATL1 facilitates fusion using an amphipathic helix (45). The tailless mutant of ATL1, when expressed at endogenous levels using *SEY1* promoter, failed to rescue the ER morphology defects in *sey1Δyop1Δ* cells (Fig. 2*B*). Thus, we tested the function of MFN-CT by tail swapping. As expected, the addition of MFN1-CT (tailless-CTM) partially rescued the defective ATL1 tailless mutant and maintained proper ER morphology (Fig. 2*B*; see Fig. S5*A* for expression levels). Notably, neither WT ATL1 nor ATL tailless containing mutants was able to restore mitochondria morphology in MFN1-deleted MEF cells (Fig. S3), consistent with their localization on the ER. These results indicate that the CTM is exchangeable with the CTA.

To further test whether chimeras containing MFN1 mediate functional ER fusion, we monitored their activities in a cell proliferation assay. Previously, it was reported that cells either lacking Sey1p or carrying *ufe1-1* mutation, a temperature-sensitive allele of the essential ER SNARE Ufe1p, grow normally, but the combination of the two mutants causes very severe growth defects (38). As expected, the expression of human ATL1, but not the

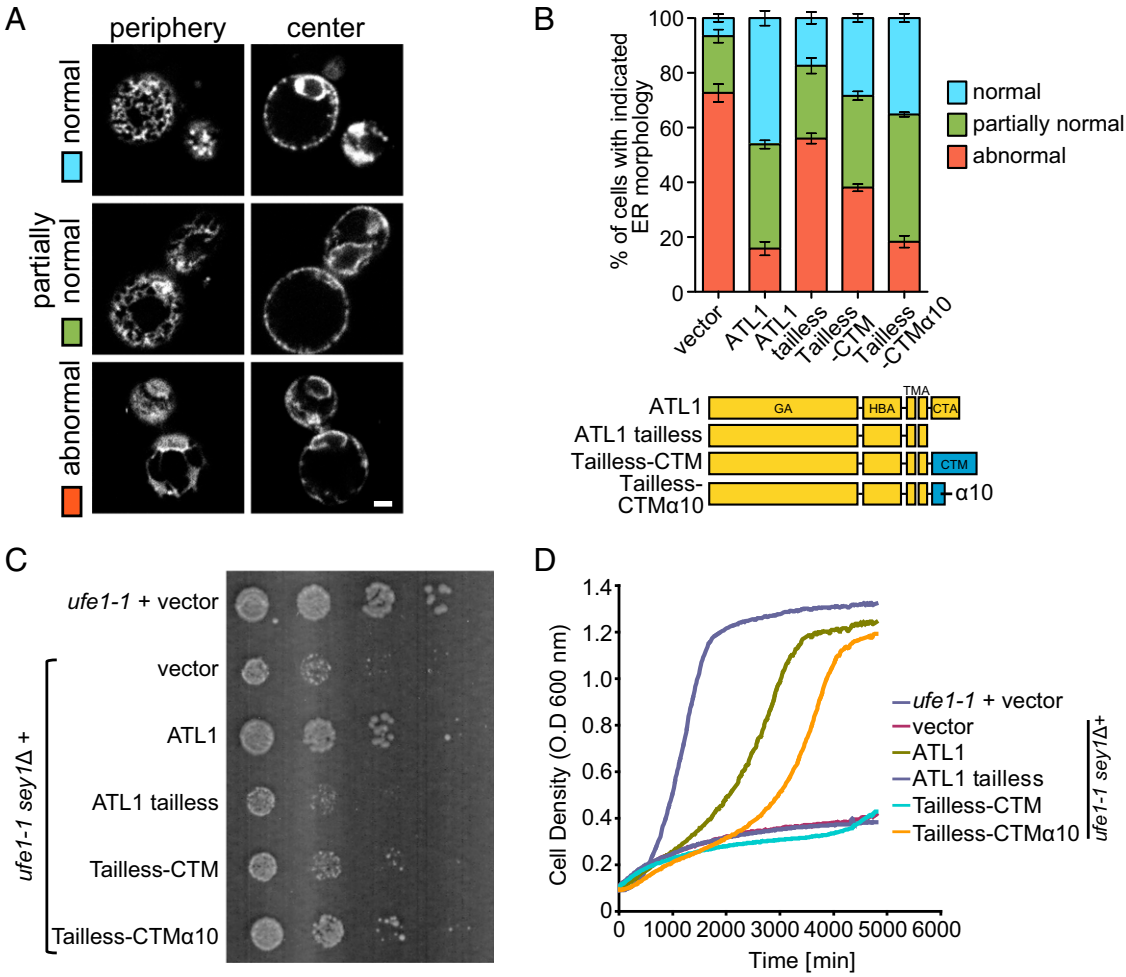

Fig. 2. Functional analysis of MFN-ATL chimeras in yeast cells. (*A*) A GFP fusion protein containing the ER protein Sec63p was expressed in yeast cells lacking Sey1p and Yop1p (*sey1Δyop1Δ* cells). The ER morphology represented by the Sec63p-GFP signal was visualized by confocal microscopy, with the microscope focused on either the center or the periphery of the cell. ER morphology was categorized into three classes. Note that the partially abnormal class exhibits some fenestrated ER but is void of ER in some areas at the periphery of the cell. (Scale bar: 1 μm.) (*B*) Empty vector or indicated chimeras were expressed with a CEN plasmid under the control of the endogenous SEY1 promoter in *sey1Δyop1Δ* cells. See Fig. S5 for expression levels and localization of the chimeras. The ER morphology was determined as in *A*, and each category was colored as in *A*. A total of 80 to 150 cells were categorized for each sample. The experiments, performed in a blinded manner, are averages of three repetitions. (*C*) The same chimeras as in *B* were transformed into *ufe1-1sey1Δ*, and empty vector was transformed into *ufe1-1* or *ufe1-1sey1Δ*. Serial 10-fold dilutions of cells were spotted onto an SC medium and incubated at 30 °C for 3 to 4 d. (*D*) Growth rates of the same cells as in *C* were determined by measuring OD600.

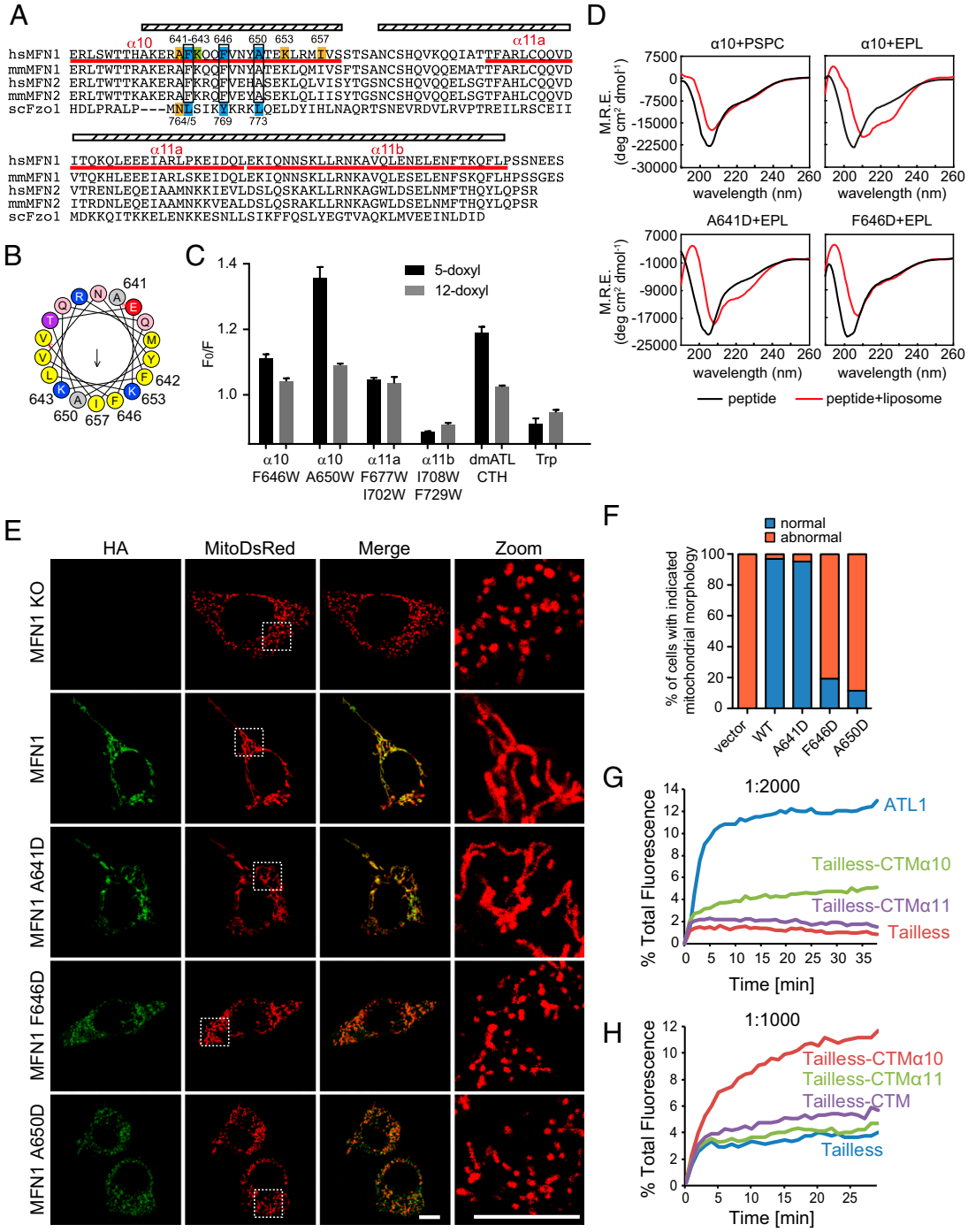

Fig. 3. An amphipathic helix in the MFN1-CT. (*A*) Sequence alignment of the CTs from various MFNs. The predicted and observed α-helices of MFN1 are labeled with cylinders. The sequences of three synthetic peptides used in this figure are underlined in red. Mutated residues are numbered, with critical ones in cyan, moderately critical ones in green, and noncritical ones in yellow. The conservation of the important residues is highlighted in black boxes. (*B*) Helical wheel representation of α10 was generated using program HeliQuest (heliquest.ipmc.cnrs.fr/). Hydrophobic, negatively charged, and positively charged residues are shown in yellow, red, and blue, respectively. Mutated residues are numbered. (*C*) Indicated peptides were added to liposomes with or without PC containing doxyl groups at position 5 or 12 of the hydrocarbon. The quenching of the fluorescence of Trp in the peptide was measured and expressed as F_0/F (maximal fluorescence with doxyl-free liposomes divided by maximal fluorescence with doxyl-containing ones). *Dm*ATL CTH is a positive control, and amino acid Trp is a negative control. Data shown are the mean and SE of three experiments. (*D*) Circular dichroism spectra of indicated peptides were recorded in the absence (black lines) or presence (red lines) of liposomes. EPL, liposomes made of *E. coli* polar lipids; M.R.E., mean residue ellipticity; PCPS, liposomes made of PC:PS (mole percent 85:15). (*E*) HA-tagged WT MFN1 or indicated mutants were transfected into MFN1-deleted MEF cells. Their localization was determined by anti-HA antibodies (green) and compared with that of MitoDsRed, a mitochondrial targeted marker protein, using indirect immunofluorescence and confocal microscopy. The right panels show the 4.7× enlargement of the indicated areas. (Scale bars: 10 μm.) (*F*) The mitochondrial morphology of indicated samples was categorized as "normal" or "abnormal". A total of 100 to 120 cells were counted for each sample. All graphs are representative of at least three repetitions. (*G*) Full-length *dm*ATL, ATL tailless, tailless-CTMα10, and tailless-CTMα11 were purified and reconstituted into donor and acceptor vesicles at a 1:2,000 protein-to-lipid ratio. GTP-dependent fusion of donor and acceptor vesicles was monitored by the dequenching of an 7-nitro-2-1,3-benzoxadiazol-4-yl (NBD)-labeled lipid present in the donor vesicles. All reactions were initiated by addition of GTP. (*H*) As in *G*, with indicated constructs tested at a 1:1,000 protein-to-lipid ratio.

tailless mutant, efficiently rescued the poor growth of the *ufe1-1sey1Δ* cells (Fig. 2*C*). When ATL tailless-CTM was tested, the growth was slightly restored (Fig. 2*C*), which is consistent with the results of the ER morphology assay. The same results were obtained when cell proliferation was measured using an automated growth curve system (Fig. 2*D*). These results support the notion that the MFN-CT is functionally analogous to, although less efficient than, ATL1-CT in facilitating membrane fusion.

An Amphipathic Helix in the MFN-CT Facilitates Fusion and Localization. The CT of ATL forms an amphipathic helix that inserts into the membrane and perturbs the lipid bilayer without causing significant lysis. Because the CT of MFN1 can partially replace the CT of ATL, we investigated whether a similar amphipathic helix is present in the MFN1-CT. Helical wheel analysis revealed that the first helix in the CT (α10) exhibited an amphipathic pattern (Fig. 3 *A* and *B*). The second helix (α11) can form a coiled coil structure (34), which requires hydrophobic residues to point in the same direction, and as such is naturally amphipathic.

We synthesized three peptides corresponding to sequences of the helical region in the MFN1-CT (α10 peptide, residues 629 to 659; α11a peptide, residues 676 to 705; and α11b peptide, residues 706 to 735) and tested whether they insert into the lipid bilayer as reported with other amphipathic helices (45). If the hydrophobic surface of an amphipathic helix contains a tryptophan (Trp), upon membrane insertion, the Trp residue would come into contact with the hydrophobic tails of lipids. The fluorescence of Trp can be quenched by doxyl groups conjugated to the hydrocarbon chains. Not all of the peptides contain Trp; thus, we replaced residues in the predicted hydrophobic faces with Trp (α10 peptide, F646W or A650W; α11a peptide, F677W/I702W; α11b peptide, I708W/F729W). To determine whether substitution with Trp affects the function of MFN1, we transfected COS-7 cells with F646W or A650W. Similar to WT MFN1, both mutants aggregated mitochondria in the perinuclear region (Fig. S6*A*) and were able to restore mitochondrial morphology in MFN1-deleted MEF cells (Fig. S6*B*), suggesting that the Trp mutants are functional. In a doxyl-quenching assay, we observed direct contact of Trp residues with membranes only when the α10 peptide was used (Fig. 3*C*). The quenching was more prominent with 5-doxyl than 12-doxyl, suggesting shallow insertion (Fig. 3*C*). Similar quenching was observed with a peptide from the equivalent amphipathic helix in the ATL-CT from *Drosophila*, but not with free Trp (Fig. 3*C*). Taken together, the results indicate that the α10 of MFN1, which forms an amphipathic helix that inserts into the membrane, may be functionally analogous to the CT of ATL.

Circular dichroism (CD) measurements provided further evidence of an interaction between the amphipathic helix and lipids. The α10 peptide corresponding to the WT sequence became more helical in the presence of liposomes (Fig. 3*D*). Helical structures appeared when *Escherichia coli* polar lipids (EPLs), a lipid mixture that is partly similar to the membrane composition of mitochondria, were used to generate liposomes, but not when phosphatidyl-choline (PC)/phosphatidyl-serine (PS) was used (Fig. 3*D*). F646D and A650D, mutations in the hydrophobic face of the first half helix, abolished the interactions and exhibited no helical folding, even in the presence of liposomes, whereas I657D, a later mutation, caused no defects (Fig. 3*D* and Fig. S6*C*). The hydrophilic face of the helix appears to be less important as mutation of A641 had little effect (Fig. 3*D*). Consistently, none of the α11 peptides exhibited lipid-induced helical formation (Fig. S6*C*). To measure the helical formation of the peptides in a more physiologically relevant environment, liposomes containing a lipid mixture of outer mitochondrial membranes (51) were used. Similar to EPL-containing liposomes, α10 peptide exhibited a helical propensity in the presence of these liposomes (Fig. S6*D*). Individual lipid types were then removed one by one from the liposomes, and the CD spectrum was determined with the α10 peptide. Cardiolipin (CL) and phosphatidyl-inositol (PI) were more important than PC and phosphatidyl-ethanolamine (PE) (Fig. S6*D*), confirming the preference of more mitochondria-specific lipids by the peptide. These results show that folding of the α10 amphipathic helix is induced upon interaction with the lipid bilayer, with the first half of the helix being more important.

To directly test the function of MFN1-α10, the α10 region was attached to the ATL tailless mutant (tailless-CTMα10) instead of the entire MFN1-CT (tailless-CTM). The chimeric protein was able to rescue the ER morphology defects in *sey1Δyop1Δ* cells (Fig. 2*B*) and growth defects in *ufe1-1sey1Δ* cells (Fig. 2 *C* and *D*), equivalent to that of WT ATL1 and even better than tailless-CTM. In addition, when MFN1-α10 was linked to the *Drosophila* ATL tailless mutant, the purified reconstituted chimera protein was able to restore ∼30% of the fusion defect of the tailless mutant at a protein-to-lipid ratio of 1:2,000 (Fig. 3*G*, see Fig. S7 *A* and *B* for reconstitution controls). Conversely, fusion by tailless ATL was not promoted by α11. Consistent with ER morphology and cell proliferation assays, the presence of α11 appeared to partly inhibit the activity of α10 as tailless-CTM was less competent in mediating fusion than tailless-CTMα10 (Fig. 3*H*). These results suggest that the α10 amphipathic helix of MFN1 is capable of facilitating ATL-mediated fusion.

To further probe the function of the amphipathic helix, we tested the effect of point mutations on MFN-mediated mitochondrial fusion using MFN1-deleted MEF cells. As shown previously, expression of WT MFN1 rescued the mitochondria fragmentation in these cells, but expression of F642D, F646D, and A650D, the hydrophobic face mutants, failed to do so (Fig. 3 *E* and *F* and Fig. S7*D*). Consistent with CD measurements, mutation A641D did not affect the function of MFN1 (Fig. 3 *E* and *F*). Based on the helical wheel prediction, both K643 and K653 flank the hydrophobic face. Mutation of K643D, the former lysine, but not K653D, reduced the ability of MFN1 to maintain mitochondrial fusion (Fig. S7*D*). Similarly, I657D, a mutant that exhibited unaltered lipid association (Fig. S6*C*), restored the mitochondrial morphology to that of WT protein (Fig. S7*D*). These results confirm that the α10 amphipathic helix is critical for MFN1 function in maintaining mitochondrial morphology in cells.

We noticed that some F646D and A650D proteins did not localize to the mitochondria (Fig. 3*E*). To test whether the amphipathic helix plays a role in MFN1 localization, we expressed HA-tagged WT or mutant MFN1 in COS-7 cells. Consistent with previous observations, overexpressed MFN1 localized to the mitochondria, causing condensation of mitochondria around the nucleus, which is likely indicative of excessive fusion (Fig. 4*A*). When the hydrophobic face of the amphipathic helix was disrupted (F642D, F646D, and A650D), some of the mutant proteins diffused into the cytosol (Fig. 4*A* and Fig. S7*E*). These mutants also failed to cause hyperfusion of the mitochondria. In contrast, the hydrophilic surface mutant A641D behaved like the WT protein; it localized to the mitochondrial membranes and its overexpression resulted in perinuclear condensation of the mitochondria (Fig. 4*A*). The localization of additional mutants (K643D, K653D, and I657D) correlated with their ability to maintain mitochondrial morphology (Fig. S7*E*). These results indicate that the α10 amphipathic helix plays a dual role facilitating mitochondrial targeting and fusion by MFN1.

α7α8 Loop Facilitates Mitochondrial Targeting of MFN. The role of the α10 amphipathic helix in MFN1 localization explains the deletion of MFN1-CT causing mistargeting. Next, we investigated how the HB region is involved in mitochondrial targeting as the mutant lacking the HB domain exhibited the same defects (Fig. S4*B*). Bacterial dynamin-like protein (BDLP) has been reported

to use a paddle domain and a loop in the trunk region to insert into membranes (52) (Fig. 4*B*). The paddle of BDLP is reminiscent of the predicted transmembrane hairpin of MFN1, and the loop region consists of three short amphipathic helices. We hypothesize that a corresponding loop in the HB domain (equivalent to the trunk domain of BDLP) that connects α7 and α8, and as such is in proximity to the lipid bilayer, plays a role in mitochondrial membrane targeting of MFN1. Helical wheel analysis of the loop revealed a less typical amphipathic character (Fig. 4*C*). Nevertheless, two conserved Phe residues were found on one side of the helical wheel. We replaced F427 and F431 with Asp and tested the mutants in COS cells. As predicted, the mutated MFN proteins partly localized to the cytosol (Fig. 4*D*). Interestingly, unlike α10 mutants, the properly targeted F427D and F431D proteins were able to aggregate mitochondria around the nucleus. These results suggest that the α7α8 loop affects localization of MFN1 via membrane insertion of bulky hydrophobic residues but is less likely to be involved in regulating fusion activity.

TM-Flanking Elements Are Conserved in Fzo1p. To test if the TM-flanking elements identified in MFN are conserved in eukaryotes, we analyzed the sequence of Fzo1p, the yeast homolog of MFN. The overall predicted secondary structure was conserved between Fzo1p and MFNs (Fig. S1). In the CT of Fzo1p, a predicted helix (755 to 775) that is equivalent to α10 in MFN1 is present immediately following the TM regions, and in the predicted α7α8 loop of Fzo1p, Y552, and Y555 are weakly equivalent to F427 and F431 in human MFN1 (Fig. 4*C* and Fig. S1). The structures of the α10 regions in MFN1 and Fzo1p were modeled using RaptorX (raptorx.uchicago.edu/StructurePrediction/predict/). Residues 631 to 657 of MFN1 were modeled as α-helical (Fig. S7*C*), which is consistent with the second half of the α10 peptide being less important. In addition, the model revealed that F642, F646, and A650 form a hydrophobic patch that faces one direction (Fig. S7*C*). Similarly, residues 763 to 775 of Fzo1p were modeled as a helix, with L765, Y769, and L733 being the hydrophobic face (Fig. S8*A*). These analyses suggest that the elements used by MFN1 for membrane targeting and fusion are likely conserved in Fzo1p.

To test whether residues found in Fzo1p are critical for maintaining proper mitochondrial morphology, we expressed WT and mutant Fzo1p under control of the endogenous *FZO1* promoter (Fig. S8*B*) in *fzo1Δ* cells and monitored mitochondrial morphology using a mitochondria-targeted GFP marker (mito-GFP). As previously reported (6), deletion of Fzo1p caused the fragmentation of mitochondria, and reintroduction of WT Fzo1p restored the ribbon-like morphology (Fig. S8*C*). Mutations in the α7α8 loop (Y552D and Y555D) and the hydrophilic face of α10 (N764D) did not compromise mitochondrial morphology, but mutations in the hydrophobic face of α10 (L765D, Y769D, and L773D) did (Fig. S8*D*). Notably, previous studies confirmed the role of α10 residues in supporting cell proliferation (53); Y769P and L773P (within the predicted α10) are inactive, but mutations of later leucines cause no defects. To further investigate the membrane targeting of Fzo1p mutants, we performed a membrane sedimentation assay. Mutations in hydrophobic residues in both the α7α8 loop and α10 helix affected the membrane targeting of Fzo1p (Fig. S8*E*). These results suggest that Fzo1p utilizes similar hydrophobic residues as MFN for proper localization and function.

Discussion

Our results provide important insights into the mechanism underlying MFN-mediated homotypic fusion of the outer mitochondrial membranes. We show that this dynamin-like GTPase is capable of mediating membrane fusion outside of mitochondria, suggesting that it is a bona fide fusogen without the requirement of mitochondria-specific cofactors. The domains of MFN protein, especially the CT, play similar roles as those of ATL.

The GTPase domain of MFN1 appears to be longer than previously estimated (48), based on a comparison with cytATL1, which is consistent with MFN having an extra HB associating with its GTPase (35, 36). Secondary structure prediction and structural analogy with BDLP suggest that the region between the GTPase and TM domain of MFN is likely an HB, similar to ATL. Finally, MFN is predicted to have one hydrophobic segment that may be a TM domain. Given that both the N and C termini are cytosolic (48), the TM segments of MFN1 likely form a hairpin without traversing the bilayer completely. The short TM domain compared with ATL implicates an additional mechanism for membrane targeting.

The fusion activities of many other membrane fusogens, including SNAREs and ATL proteins, have been demonstrated in vitro using reconstituted vesicles containing purified proteins (54). Such direct evidence has not been reported for MFN. In vitro fusion assays using isolated mitochondria have shown that the MFN family is necessary for fusion of the outer mitochondrial membranes (55). However, several important mitochondria-related factors, including inner membrane potentials and mitochondria-resident proteins, such as outer membrane protein Ugo1p (56), can drastically affect MFN- or Fzo1p-mediated fusion, which prevents the conclusion that MFN may act alone for fusion. Here, we showed that, when MFN1 is relocated to the ER using the ATL1-TM domain (chimera A1), it can replace ER fusogen Sey1p in maintaining ER morphology and mediate ER fusion in yeast cells. The partial restoration of ER morphology was likely caused by low and uneven levels of A1 expression among the tested cells. Alternatively, the previously reported regulatory proteins for MFN family members are needed to boost the activity of these fusogenic proteins to a necessary level. Nevertheless, our evidence favors the notion that MFN is intrinsically capable of mediating membrane fusion.

In addition to the GTPase, we showed that the HB of MFN1 is indispensable. Based on recent structural studies (35, 36), HBM is likely complemented by the first half of HR2 (α11a), mimicking the configuration of the trunk domain of BDLP. In ATL, the stalk-like HB relays the conformational changes initiated in the GTPase domain to the TM domain and embedded membrane. Whether HBM moves similarly remains to be investigated.

The TM domains of both ATL and MFN likely form hairpin structures. In the case of ATL, the two TMs are in very close proximity, and the MFN-TM domain may not even cross the membrane completely, representing an extreme case of hairpin structure. The short TMM is consistent with the mitochondrial membranes being thinner than other cellular membranes (57), and the TM helices of mitochondrial membrane proteins are relatively short (58). TM hairpins are commonly found in proteins that prefer high curvature of the lipid bilayer (59, 60). Because the outer surface of a mitochondrion is not as bent as that of ER tubules, it is possible that the hairpin configurations of the TM domains may be useful in other aspects, probably related to the fusion process. We previously demonstrated that the ATL-TM domain is not exchangeable with other TM domains (45). Similarly, we would predict that the MFN-TM domain is sequence-specific. However, when the ATL1-TM domain is used by MFN1 (chimera A1), it appears to be active. In addition, both TMs mediate oligomerization independently of nucleotide (45), suggesting the existence of some unknown features of the TM domains shared by these proteins.

The most intriguing results for MFN fusion are due to its CT, which includes a previously characterized HR2 fragment. Our results indicate that the MFN-CT, particularly the α10 helix, is functionally equivalent to the ATL-CT, which is known to form an amphipathic helix that binds to, and destabilizes, the lipid

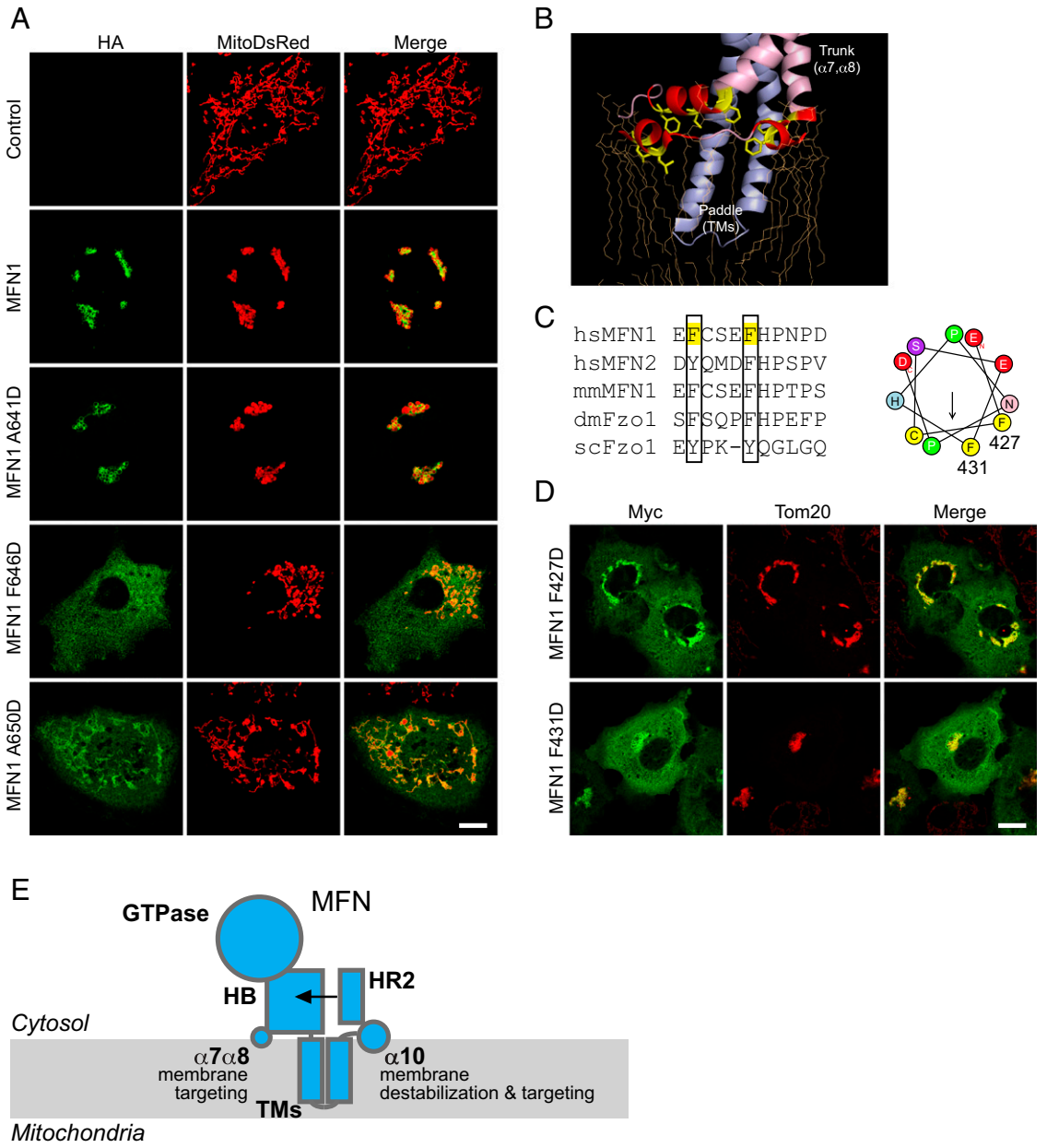

Fig. 4. TM-flanking sequences that support MFN1 targeting. (*A*) COS-7 cells were transfected with HA tagged WT MFN1 or indicated mutants. Their localization was determined by anti-HA antibodies (green) and compared with that of MitoDsRed using indirect immunofluorescence and confocal microscopy. (Scale bar: 10 μm.) (*B*) The membrane interacting regions of BDLP (PDB ID code 2W6D) are shown in schematic representation. Lipids are shown in yellow sticks. (*C*) Sequence alignment of the loop between α7 and α8. The conserved residues are highlighted with black boxes. (*Right*) The helical wheel representation of the loop generated using HeliQuest. (*D*) As in *A*, but with cells expressing Myc-tagged mutants in the α7 and α8 loop. Their localization was determined by anti-Myc antibodies (green) and compared with that of Tom20 (red), a mitochondrial membrane protein, using indirect immunofluorescence and confocal microscopy. (Scale bar: 10 μm.) (*E*) Domain functions of MFN. MFN is shown in cyan. The proposed function of each domain is indicated. HB, helix bundle; HR2, heptad repeat 2; TM, transmembrane domain; α7α8, loop connecting α7 and α8.

bilayer (45). The remaining region of the MFN-CT was previously proposed to mediate homo-dimer formation in an antiparallel manner. Given the large hydrophobic face of the long helix, dimerization is plausible when it is isolated from its molecular context. Another likely scenario is that this helix compliments the HB domain in the N terminus, as suggested by intramolecular interaction analysis (60, 61) and MGD structures (36). Alternatively, it may form a binding platform for molecules associated with MFN. HR2 has been proposed to be released during the actions of MFN because peptides derived from HR1 could regulate MFN-mediated fusion and even normalize mitochondrial morphology defects caused by CMT2A mutants (62). However, when dislocated from HR1, HR2 may gain tethering activity, as seen in the HR2 structure. In peptide-treated cells, only the appearance of the mitochondria was assessed. Whether mitochondria are functional remains to be tested. Furthermore, our results suggest that unchecked HR2, when attached to ATL tailless and lacking an intramolecular binding partner, exhibits inhibitory effects on fusion. Mutations or modifications in the HR2 region, such as oxidation of C684 in MFN2 (63), have also been demonstrated

to cause functional defects. Nevertheless, these results could be interpreted alternatively as subsequent folding defects of the mutations.

Our mechanistic probing of MFN1 demonstrates the dependence of each domain and the specific role of the CT in mediating membrane fusion (Fig. 4*E*). It also provides insight into the molecular determinants of the localization of MFN1. The combination of the α7α8 loop, the α10 helix, and the relatively short TM hairpin stabilizes MFN1 on membranes (Fig. 4*E*). The amphipathic nature of the TM-flanking regions is less typical than other known amphipathic helices, in that the hydrophobic face is relatively small. However, their membrane engagement is facilitated by the presence of the TM hairpin nearby. Our results offer an explanation for previous observations that both sides of the TM domain are important for the localization of MFN1. The mechanism proposed for MFN1 could apply to MFN2, Fuzzy Onion, Fzo1p, and their homologs in the fusion of mitochondrial outer membranes in different tissues or species. Thus, the chimeras generated here offer opportunities for investigating how the MFN family is regulated and for in vitro studies with purified components.

Materials and Methods

Mammalian Cell Culture, Transfection, and Confocal Microscopy. MEF cells and COS-7 cells were maintained at 37 °C in 5% CO_2. Transfections were performed using Lipofectamine 3000 or Lipofectamine 2000 (Invitrogen) according to the manufacturer's instructions. Confocal imaging was performed as described previously (36, 39).

Fluorescence Microscopy in Yeast. Yeast cells were cultured and visualized as previously described (39).

Circular Dichroism. Liposomes used for CD measurements were made of 85:15 mol percent POPC:DOPS, 50:30:10:10 mol percent POPC:PE:PI:CL, or EPLs (Avanti Polar Lipids) and extruded through filters with 100-nm pores. Peptides and the indicated liposomes were mixed to final concentrations of 60 μM and 2 mM, respectively, in 10 mM potassium phosphate and 100 mM KCl (pH 7.5). Spectra were collected as described previously (45).

Doxyl-Quenching Assay. Liposomes used for the doxyl-quenching assay were prepared from EPLs, with or without doxyl-PC (Avanti Polar Lipids). Peptides and the indicated liposomes were mixed to final concentrations of 20 μM and 400 μM, respectively, in 10 mM potassium phosphate and 100 mM KCl (pH 7.5). Trp fluorescence was measured as described previously (45).

In Vitro Fusion Assay. Lipid-mixing assays were performed as described previously (42).

Further details on methods are provided in *SI Materials and Methods*.

ACKNOWLEDGMENTS. We thank Dr. Xin Bian, Dr. Guo Chen, Xiaoting Wang, Jing Wang, and Ying Wang for technical assistance. J.H. is supported by National Key Research and Development Program Grant 2016YFA0500201, National Natural Science Foundation of China Grants 31630020 and 3142100024, and an International Early Career Scientist grant from the Howard Hughes Medical Institute.

1. Detmer SA, Chan DC (2007) Functions and dysfunctions of mitochondrial dynamics. *Nat Rev Mol Cell Biol* 8:870–879.
2. Hoppins S, Nunnari J (2009) The molecular mechanism of mitochondrial fusion. *Biochim Biophys Acta* 1793:20–26.
3. Youle RJ, van der Bliek AM (2012) Mitochondrial fission, fusion, and stress. *Science* 337:1062–1065.
4. Praefcke GJ, McMahon HT (2004) The dynamin superfamily: Universal membrane tubulation and fission molecules? *Nat Rev Mol Cell Biol* 5:133–147.
5. Santel A, Fuller MT (2001) Control of mitochondrial morphology by a human mitofusin. *J Cell Sci* 114:867–874.
6. Hermann GJ, et al. (1998) Mitochondrial fusion in yeast requires the transmembrane GTPase Fzo1p. *J Cell Biol* 143:359–373.
7. Rapaport D, Brunner M, Neupert W, Westermann B (1998) Fzo1p is a mitochondrial outer membrane protein essential for the biogenesis of functional mitochondria in Saccharomyces cerevisiae. *J Biol Chem* 273:20150–20155.
8. Meeusen S, et al. (2006) Mitochondrial inner-membrane fusion and crista maintenance requires the dynamin-related GTPase Mgm1. *Cell* 127:383–395.
9. Olichon A, et al. (2003) Loss of OPA1 perturbates the mitochondrial inner membrane structure and integrity, leading to cytochrome c release and apoptosis. *J Biol Chem* 278:7743–7746.
10. Smirnova E, Griparic L, Shurland DL, van der Bliek AM (2001) Dynamin-related protein Drp1 is required for mitochondrial division in mammalian cells. *Mol Biol Cell* 12: 2245–2256.
11. Hales KG, Fuller MT (1997) Developmentally regulated mitochondrial fusion mediated by a conserved, novel, predicted GTPase. *Cell* 90:121–129.
12. Chen H, Chan DC (2005) Emerging functions of mammalian mitochondrial fusion and fission. *Hum Mol Genet* 14:R283–R289.
13. Chen H, et al. (2003) Mitofusins Mfn1 and Mfn2 coordinately regulate mitochondrial fusion and are essential for embryonic development. *J Cell Biol* 160:189–200.
14. Ishihara N, Eura Y, Mihara K (2004) Mitofusin 1 and 2 play distinct roles in mitochondrial fusion reactions via GTPase activity. *J Cell Sci* 117:6535–6546.
15. Züchner S, et al. (2004) Mutations in the mitochondrial GTPase mitofusin 2 cause Charcot-Marie-Tooth neuropathy type 2A. *Nat Genet* 36:449–451, and erratum (2004) 36:660.
16. Kasahara A, Cipolat S, Chen Y, Dorn GW, 2nd, Scorrano L (2013) Mitochondrial fusion directs cardiomyocyte differentiation via calcineurin and Notch signaling. *Science* 342: 734–737.
17. Gong G, et al. (2015) Parkin-mediated mitophagy directs perinatal cardiac metabolic maturation in mice. *Science* 350:aad2459.
18. Luchsinger LL, de Almeida MJ, Corrigan DJ, Mumau M, Snoeck HW (2016) Mitofusin 2 maintains haematopoietic stem cells with extensive lymphoid potential. *Nature* 529: 528–531.
19. Zhang J, et al. (2016) GASZ and mitofusin-mediated mitochondrial functions are crucial for spermatogenesis. *EMBO Rep* 17:220–234.
20. Dietrich MO, Liu ZW, Horvath TL (2013) Mitochondrial dynamics controlled by mitofusins regulate Agrp neuronal activity and diet-induced obesity. *Cell* 155:188–199.
21. Schneeberger M, et al. (2013) Mitofusin 2 in POMC neurons connects ER stress with leptin resistance and energy imbalance. *Cell* 155:172–187.
22. Legros F, Lombès A, Frachon P, Rojo M (2002) Mitochondrial fusion in human cells is efficient, requires the inner membrane potential, and is mediated by mitofusins. *Mol Biol Cell* 13:4343–4354.
23. Leboucher GP, et al. (2012) Stress-induced phosphorylation and proteasomal degradation of mitofusin 2 facilitates mitochondrial fragmentation and apoptosis. *Mol Cell* 47:547–557.
24. Chen Y, Dorn GW, 2nd (2013) PINK1-phosphorylated mitofusin 2 is a Parkin receptor for culling damaged mitochondria. *Science* 340:471–475.
25. Cohen MM, Leboucher GP, Livnat-Levanon N, Glickman MH, Weissman AM (2008) Ubiquitin-proteasome-dependent degradation of a mitofusin, a critical regulator of mitochondrial fusion. *Mol Biol Cell* 19:2457–2464.
26. Gegg ME, et al. (2010) Mitofusin 1 and mitofusin 2 are ubiquitinated in a PINK1/parkin-dependent manner upon induction of mitophagy. *Hum Mol Genet* 19: 4861–4870.
27. Anton F, Dittmar G, Langer T, Escobar-Henriques M (2013) Two deubiquitylases act on mitofusin and regulate mitochondrial fusion along independent pathways. *Mol Cell* 49:487–498.
28. Lee JY, et al. (2014) MFN1 deacetylation activates adaptive mitochondrial fusion and protects metabolically challenged mitochondria. *J Cell Sci* 127:4954–4963.
29. Eura Y, Ishihara N, Oka T, Mihara K (2006) Identification of a novel protein that regulates mitochondrial fusion by modulating mitofusin (Mfn) protein function. *J Cell Sci* 119:4913–4925.
30. Hoppins S, et al. (2011) The soluble form of Bax regulates mitochondrial fusion via MFN2 homotypic complexes. *Mol Cell* 41:150–160.
31. Nakamura N, Kimura Y, Tokuda M, Honda S, Hirose S (2006) MARCH-V is a novel mitofusin 2- and Drp1-binding protein able to change mitochondrial morphology. *EMBO Rep* 7:1019–1022.
32. Ohba Y, et al. (2013) Mitochondria-type GPAT is required for mitochondrial fusion. *EMBO J* 32:1265–1279.
33. Zhang J, et al. (2010) G-protein β2 subunit interacts with mitofusin 1 to regulate mitochondrial fusion. *Nat Commun* 1:101.
34. Koshiba T, et al. (2004) Structural basis of mitochondrial tethering by mitofusin complexes. *Science* 305:858–862.
35. Cao YL, et al. (2017) MFN1 structures reveal nucleotide-triggered dimerization critical for mitochondrial fusion. *Nature* 542:372–376.
36. Qi Y, et al. (2016) Structures of human mitofusin 1 provide insight into mitochondrial tethering. *J Cell Biol* 215:621–629.
37. Brandt T, Cavellini L, Kühlbrandt W, Cohen MM (2016) A mitofusin-dependent docking ring complex triggers mitochondrial fusion in vitro. *Elife* 5:e14618.
38. Anwar K, et al. (2012) The dynamin-like GTPase Sey1p mediates homotypic ER fusion in S. cerevisiae. *J Cell Biol* 197:209–217.
39. Hu J, et al. (2009) A class of dynamin-like GTPases involved in the generation of the tubular ER network. *Cell* 138:549–561.
40. Orso G, et al. (2009) Homotypic fusion of ER membranes requires the dynamin-like GTPase atlastin. *Nature* 460:978–983.
41. Zhang M, et al. (2013) ROOT HAIR DEFECTIVE3 family of dynamin-like GTPases mediates homotypic endoplasmic reticulum fusion and is essential for Arabidopsis development. *Plant Physiol* 163:713–720.
42. Bian X, et al. (2011) Structures of the atlastin GTPase provide insight into homotypic fusion of endoplasmic reticulum membranes. *Proc Natl Acad Sci USA* 108:3976–3981.

43. Byrnes LJ, Sondermann H (2011) Structural basis for the nucleotide-dependent dimerization of the large G protein atlastin-1/SPG3A. *Proc Natl Acad Sci USA* 108: 2216–2221.
44. Byrnes LJ, et al. (2013) Structural basis for conformational switching and GTP loading of the large G protein atlastin. *EMBO J* 32:369–384.
45. Liu TY, et al. (2012) Lipid interaction of the C terminus and association of the transmembrane segments facilitate atlastin-mediated homotypic endoplasmic reticulum fusion. *Proc Natl Acad Sci USA* 109:E2146–E2154.
46. Yan L, et al. (2015) Structures of the yeast dynamin-like GTPase Sey1p provide insight into homotypic ER fusion. *J Cell Biol* 210:961–972.
47. Rost B, Yachdav G, Liu J (2004) The PredictProtein server. *Nucleic Acids Res* 32: W321–W326.
48. Rojo M, Legros F, Chateau D, Lombès A (2002) Membrane topology and mitochondrial targeting of mitofusins, ubiquitous mammalian homologs of the transmembrane GTPase Fzo. *J Cell Sci* 115:1663–1674.
49. Voeltz GK, Prinz WA, Shibata Y, Rist JM, Rapoport TA (2006) A class of membrane proteins shaping the tubular endoplasmic reticulum. *Cell* 124:573–586.
50. Hu J, et al. (2008) Membrane proteins of the endoplasmic reticulum induce high-curvature tubules. *Science* 319:1247–1250.
51. van Meer G, Voelker DR, Feigenson GW (2008) Membrane lipids: Where they are and how they behave. *Nat Rev Mol Cell Biol* 9:112–124.
52. Low HH, Löwe J (2006) A bacterial dynamin-like protein. *Nature* 444:766–769.
53. Griffin EE, Chan DC (2006) Domain interactions within Fzo1 oligomers are essential for mitochondrial fusion. *J Biol Chem* 281:16599–16606.
54. Weber T, et al. (1998) SNAREpins: Minimal machinery for membrane fusion. *Cell* 92: 759–772.
55. Meeusen S, McCaffery JM, Nunnari J (2004) Mitochondrial fusion intermediates revealed in vitro. *Science* 305:1747–1752.
56. Hoppins S, Horner J, Song C, McCaffery JM, Nunnari J (2009) Mitochondrial outer and inner membrane fusion requires a modified carrier protein. *J Cell Biol* 184:569–581.
57. Pelttari A, Helminen HJ (1979) The relative thickness of intracellular membranes in epithelial cells of the ventral lobe of the rat prostate. *Histochem J* 11:613–624.
58. Pogozheva ID, Tristram-Nagle S, Mosberg HI, Lomize AL (2013) Structural adaptations of proteins to different biological membranes. *Biochim Biophys Acta* 1828: 2592–2608.
59. Park SH, Zhu PP, Parker RL, Blackstone C (2010) Hereditary spastic paraplegia proteins REEP1, spastin, and atlastin-1 coordinate microtubule interactions with the tubular ER network. *J Clin Invest* 120:1097–1110.
60. Shnyrova A, Frolov VA, Zimmerberg J (2008) ER biogenesis: Self-assembly of tubular topology by protein hairpins. *Curr Biol* 18:R474–R476.
61. Huang P, Galloway CA, Yoon Y (2011) Control of mitochondrial morphology through differential interactions of mitochondrial fusion and fission proteins. *PLoS One* 6: e20655.
62. Franco A, et al. (2016) Correcting mitochondrial fusion by manipulating mitofusin conformations. *Nature* 540:74–79.
63. Shutt T, Geoffrion M, Milne R, McBride HM (2012) The intracellular redox state is a core determinant of mitochondrial fusion. *EMBO Rep* 13:909–915.